

River, tide and morphology interaction in a macro-tidal estuary with active morphological evolutions

Xie, Dongfeng; Bing Wang, Zheng; Huang, Junbao; Zeng, Jian

DOI

[10.1016/j.catena.2022.106131](https://doi.org/10.1016/j.catena.2022.106131)

Publication date

2022

Document Version

Accepted author manuscript

Published in

Catena

Citation (APA)

Xie, D., Bing Wang, Z., Huang, J., & Zeng, J. (2022). River, tide and morphology interaction in a macro-tidal estuary with active morphological evolutions. *Catena*, 212, Article 106131. <https://doi.org/10.1016/j.catena.2022.106131>

Important note

To cite this publication, please use the final published version (if applicable). Please check the document version above.

Copyright

Other than for strictly personal use, it is not permitted to download, forward or distribute the text or part of it, without the consent of the author(s) and/or copyright holder(s), unless the work is under an open content license such as Creative Commons.

Takedown policy

Please contact us and provide details if you believe this document breaches copyrights. We will remove access to the work immediately and investigate your claim.

1 **River, tide and morphology interaction in a macro-tidal estuary with active**

2 **morphological evolutions**

3 Dongfeng Xie¹, Zheng Bing Wang^{2,3}, Junbao Huang¹, Jian Zeng¹

4 1 Zhejiang Institute of Hydraulics and Estuary, Hangzhou, China.

5 2 Faculty of Civil Engineering and Geosciences, Delft University of Technology, Delft, the

6 Netherlands.

7 3 Deltares, Delft, the Netherlands.

8

9 **Corresponding author at:**

10 Zhejiang Institute of Hydraulics and Estuary, Hangzhou 310020, China

11 **Email address:** dongfeng.xie@hotmail.com (D. Xie).

12

13 **Abstract:** Understanding tidal dynamics in estuaries is essential for tidal predictions and
14 assessments of sediment transport and associated morphological changes. Most studies on
15 river-tide interaction ignored the influences of morphological evolutions under natural conditions
16 such as the seasonal and interannual variations of river discharge. This study analyzes the
17 multiple-timescale tidal dynamics in the Qiantang Estuary, a macro-tidal estuary in China with an
18 extremely active morphological evolution. A large dataset including water levels at representative
19 stations, river discharges and bathymetries since 1980 has been collected. The results of the
20 analysis show that within a spring-neap cycle, the tidal amplification in the upper estuary is
21 stronger during spring tide than during neap tide. This unexpected behavior is due to the high
22 sediment concentration and the unique longitudinal profile of the estuary. On the seasonal and
23 interannual timescales, the low water levels in the upper estuary depend on the local bathymetrical
24 conditions. Tidal ranges in the upper estuary are larger in the high flow season and years, than in
25 the low flow season and years, due to the erosion at high flow, in contrast to estuaries with less
26 active morphological changes. During low flow season and years, the bed is gradually recovered,
27 the low waters are elevated, and the tidal ranges decrease accordingly. A good relationship exists
28 between the tidal ranges and the depth of the upper estuary. In the lower estuary, the flood
29 dominance increases continuously due to embankment. In the upper estuary, the flood dominance
30 is increased during the high flow periods, explaining the fast sediment input and bed recovery in
31 the post high flow periods. A conceptual model of river-tide-morphology interaction of the estuary
32 is proposed, which is also applicable for other shallow systems.

33 **Key words:** Tidal dynamics; River discharge; Tidal amplification; Morphological evolution;
34 Qiantang Estuary.

35 **1. Introduction**

36 Estuaries, transitional zones where a river meets the open sea, are worldwide surrounded
37 by densely populated areas subject to fast economic development ([Syvitski et al., 2009](#)).
38 Understanding tidal wave propagation and the corresponding spatial-temporal variations of
39 the tide in estuaries is essential for tidal predictions and assessments of sediment transport and
40 associated morphological changes. Water levels are probably the easiest data to measure in an
41 estuary, and often the only oceanographic data available that extend back to time periods
42 before the 20th century. They contain important information about the estuary and, therefore,
43 implicitly provide a history of environmental change ([Wang et al., 2019](#); [Talke and Jay, 2019](#)).
44 From a coastal management point of view, they are of major practical significance for
45 navigation, flood defense and provide information on salt intrusion and the estuarine
46 ecosystem ([Friedrichs and Aubrey, 1994](#); [Kulkuka and Jay, 2003](#); [Jay et al., 2011](#); [Hoitink and](#)
47 [Jay, 2016](#); [Talke and Jay, 2019](#)).

48 Although many studies have evaluated tidal distortion in different estuaries (e.g.,
49 [Dronkers, 1986](#); [Friedrichs and Aubrey, 1988](#); [Wang et al., 2002](#); [Bolle et al., 2010](#); [Toublanc](#)
50 [et al., 2015](#)), river-tide interactions, mostly based on analytical or numerical models, have
51 only recently gained attention, including Changjiang (Yangtze) River estuary and Pearl River
52 estuary in China ([Guo et al., 2015, 2019](#); [Cai et al., 2015, 2020](#)). Water level dynamics within
53 estuaries are subject to various external forcing factors, such as basin geometry (length,
54 convergence in width and bathymetry), river discharge influenced by hydrological variations
55 in catchment areas, and oceanic tides. Depending on the balance between bed friction,
56 estuarine convergence and river discharge, the incoming tides experience amplification,

57 damping or remain constant in amplitude (Jay, 1991; Savenije, 2012). River discharge is
58 rarely constant and can vary rapidly over a large range, which induces a highly nonstationary
59 behavior of tides in estuaries, especially into the landward direction (Guo et al., 2015; Jay et
60 al., 2011; Kukulka and Jay, 2003a, b). A higher river discharge dissipates tidal energy, slows
61 down tidal wave propagation and reduces the tidal range by enhanced bed friction (Godin,
62 1991; Cai et al., 2012; Zhang et al., 2015a). The river-tide interaction causes a higher mean
63 water level during spring tide than during neap tide, explaining the fortnightly oscillations in
64 mean water level (Matte et al., 2014). Most studies on river-tide interactions ignored the
65 influences of morphological evolutions, because the bed level change over a short-term, e.g.,
66 spring-neap tidal cycle or seasonal timescale is limited with respect to the water depth.

67 Long-term changes in bottom friction, morphology and river discharge can modify tidal
68 amplification and tidal asymmetry. Many studies have examined the long-term changes of
69 tidal properties influenced by human activities, such as sand mining, land reclamation,
70 channel deepening, bridges and weirs (Wang et al., 2002; Bolle et al., 2010; Zhang et al.,
71 2010; Cai et al., 2012; Song et al., 2013; Winterwerp et al., 2013; Talke and Jay et al., 2019).
72 However, few studies on river-tide interaction consider the influence of morphological
73 evolution under natural conditions such as the seasonal and interannual variations of river
74 discharge and tides, probably because in most estuaries the timescales of morphological
75 evolution are much larger than those of the variations of hydrodynamic conditions.

76 There are some estuaries in the world with active seasonal or interannual morphological
77 evolutions (Cooper, 2002; Shaw and Mohrig, 2014; Shimozono et al., 2019; Choi et al., 2020).
78 It is necessary to explore the influence of the fast morphological evolutions on the tidal

79 dynamics in such type of estuaries. The Qiantang Estuary, located at the East China Sea coast,
80 is a typical example of the macro-tidal estuaries with active morphological evolutions (Fig. 1).
81 The mean and maximum tidal ranges at Ganpu, the interface between the Qiantang Estuary
82 and Hangzhou Bay, are 5.62 m and 9.0 m respectively (Han et al., 2003). The estuary is
83 known for one of the strongest tidal bores worldwide. The swift tidal currents and river flood
84 events result in substantial morphological changes on seasonal and interannual timescales. In
85 several months, the local bed level changes can be more than 5 m (Chen et al., 1990; Han et
86 al., 2003). In recent years, multiple studies have been carried out on tidal bore formation,
87 propagation and turbulence properties (Pan et al., 2007; Pan and Huang, 2010; Tu and Fan,
88 2017), associated sediment transport and sedimentary sequence (Fan et al., 2014; Lin et al.,
89 2005; Zhang et al., 2015b), based on field work and numerical modeling. The most
90 remarkable morphological feature of the estuary is a large bar, a morphological bulge,
91 elongating from the middle Hangzhou Bay landwards by 130 km (Fig. 1b). Several
92 morphodynamic models have reproduced the formation of the large bar and its
93 morphodynamic response to the large-scale embankment project since the 1960s (Yu et al.,
94 2012; Xie et al., 2017a; Hu et al., 2018; Huang and Xie, 2020; Xie et al., 2021). Xie et al.
95 (2018) found that the morphodynamic equilibrium of the estuary is maintained by the
96 combination of two extreme hydrological conditions: tidal bore and river flood events. So far,
97 no study focused on the tidal dynamics in the estuary, particularly on the interaction with fast
98 morphological evolutions, has been carried out.

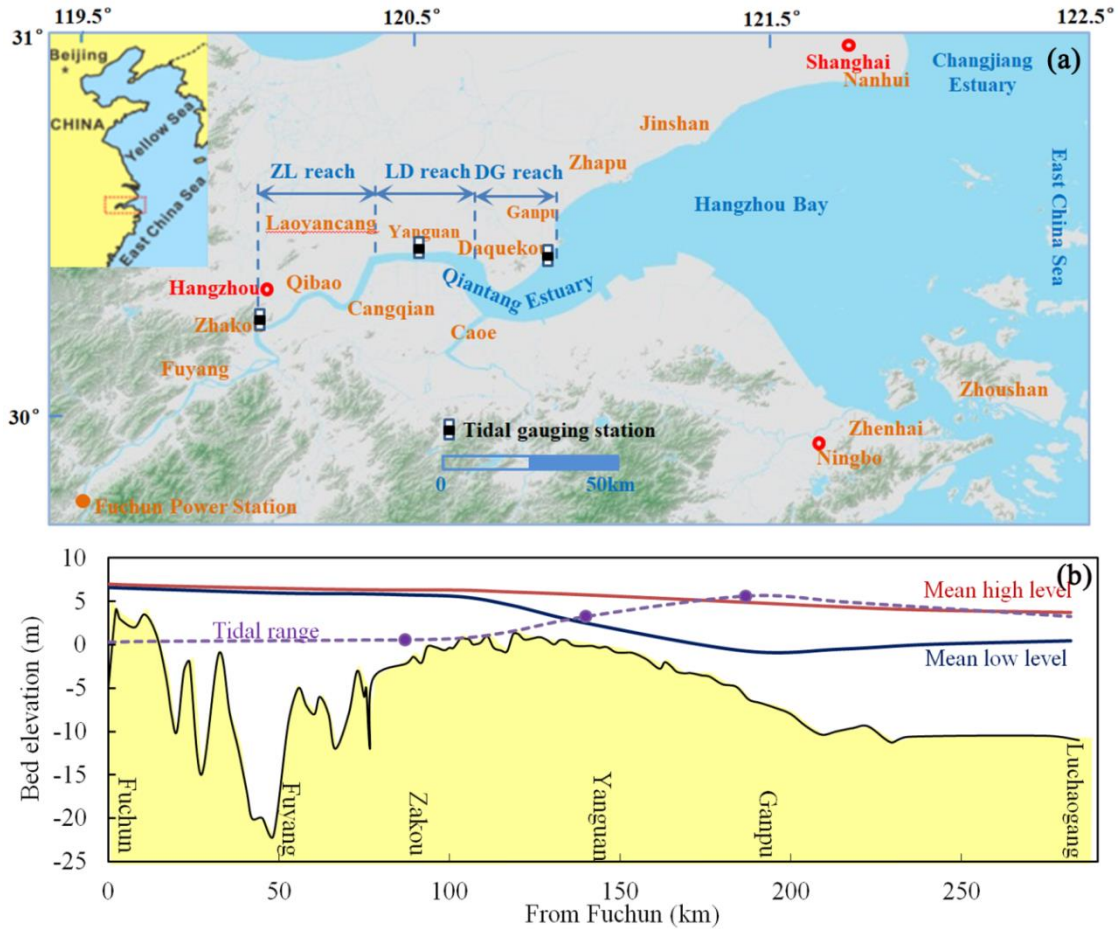
99 Based on the long-term bathymetrical data, together with data of water levels and river
100 discharges, the present study investigates the tidal dynamics in the Qiantang Estuary. Specific

101 objectives are: (1) to delineate the morphological evolutions under seasonal and interannual
102 river discharge variations; (2) to analyze spatial-temporal variations of water levels and tidal
103 amplifications on spring-neap, seasonal, annual and decadal timescales; (3) to link the tidal
104 dynamics and morphological evolutions. The findings of this study are also relevant for other
105 tidal systems with fast morphological changes.

106

107 **2. Study area**

108 With a total length of 386 km and a catchment area of about 60000 km², the Qiantang
109 River is the largest river in the Zhejiang Province, China. The river debouches into the 120
110 km - long Hangzhou Bay, which has a funnel shape with the widths decreasing from 98.5 km
111 at the bay mouth to 18.5 km at the bay head (Fig. 1a).



112

113 **Fig. 1.** (a) Location of Qiantang Estuary; (b) the lateral-averaged longitudinal bathymetries and

114 the mean high and low tidal levels and tidal range along the estuary (after Xie et al., 2017a). The

115 dots in panel b denote the locations of tidal stations of Zhakou, Yanguan and Ganpu.

116

117 The Qiantang Estuary is usually divided into two reaches according to the hydrodynamic

118 and morphological characteristics (Han et al., 2003). The riverine reach between Fuchun

119 power station and the town of Zhakou is river-dominated with limited tidal influence. With

120 the sediments mostly composed of gravel (2 - 30 mm) and coarse sand (0.05 - 0.5 mm), the

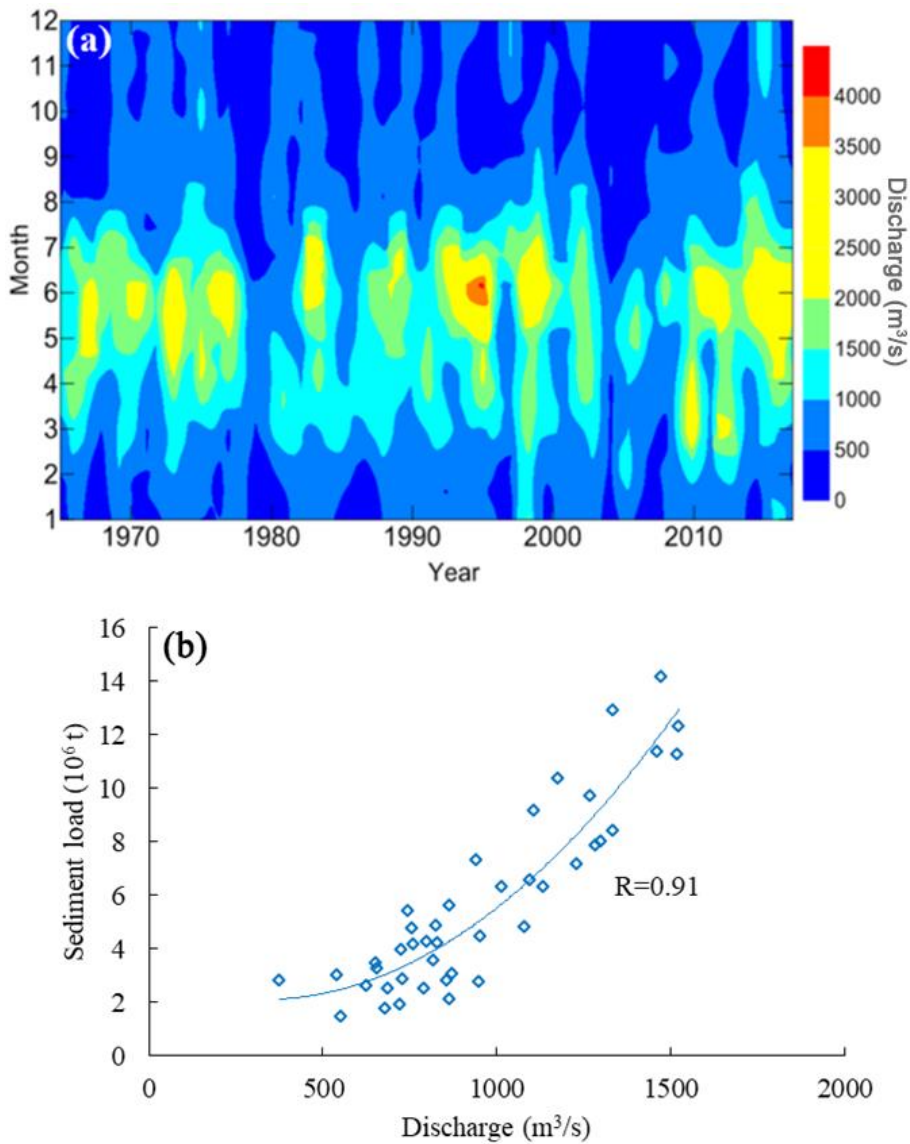
121 morphology in the riverine reach is relatively stable (Han et al., 2003; Chen et al., 2006). The

122 estuarine reach between the towns of Zhakou and Ganpu is controlled by the combination of

123 river flow and tide, sedimented with silt and clay with a median grain size of predominantly

124 0.02 - 0.04 mm (Chen et al., 1990). This reach is dominated by the main part of the large
125 longitudinal bar (Fig. 1b). The highest part of the bar is located between the towns of
126 Cangqian and Qibao. It is more than 10 m higher than the estuary bottom at both the upstream
127 and downstream sides of the bar. The Hangzhou Bay downstream of Ganpu, with an average
128 depth of around 10 m, is dominated by tidal currents and the sediments are predominantly
129 consisting of silt and clay (0.004 - 0.063 mm) (ECCHE, 1992). Tides from the East China Sea
130 are dominated by the principal lunar semi-diurnal M_2 constituent. At the Hangzhou Bay
131 mouth the mean tidal range is 3.2 m, gradually increasing landward to 5.62 m at Ganpu due to
132 the strong convergence of width in the bay.

133 The current study, we focus on the estuarine reach of the Qiantang Estuary. According to
134 the hydrographic and morphological characteristics, it can be divided into three sub-reaches.
135 From Ganpu to Daquekou (DG reach) the width decreases from 18.5 to 5 km. Mean tidal
136 range gradually decreases from 5.62 m to 3.28 m due to bed friction. It is located at the
137 seaward slope of the large bar and the bed level rises from around -5 m at Ganpu to around -1
138 m at Daquekou. As a result, the tidal wave is seriously distorted. From Daquekou to
139 Laoyancang (LD reach) the width decreases from 5 km to 2 km. The distorted tidal wave at
140 this sub-reach eventually evolves into the world-famous tidal bore, where the bore height can
141 be 1 - 2 m during spring tides (Han et al., 2003; Pan et al., 2007). From Zhakou to
142 Laoyancang (ZL reach) the width is 1 - 2 km. The bed elevation shows a landward decreasing
143 trend from 1 - 2 m to around -2 m. The tidal bore is gradually weakened and disappears. Mean
144 tidal range at Zhakou is 0.58 m.



145

146

147 **Fig. 2.** (a) Monthly averaged discharges (m³/s) and (b) annual sediment load - discharge rating

148 curve of the Qiantang River. The data were collected from Zhejiang Hydrography Bureau, China.

149

150 The mean discharge of the Qiantang River is 952 m³/s (Han et al., 2003). The monthly

151 averaged discharges vary between 319 and 1705 m³/s (Fig. 2a). The runoff mainly occurs in

152 the rainy season (between April and July), accounting for 55 - 60% of the annual runoff.

153 During a river flood event, the discharge rises and falls sharply in several or more than 10

154 days, and the peak discharge can be more than 10000 m³/s (Han et al., 2003). The flood
155 events substantially correlate with the Asian summer monsoon as well as the local climate and
156 other regional factors such as geographical variation and local sources of aerosols (Tian et al.,
157 2012; Xia et al., 2016). Furthermore, it is characterized by the alternate wet and dry years on
158 the interannual timescales, with the period around 20 years (Zeng et al., 2010). The sediment
159 load from the Qiantang River correlates with the river discharge, varying between 1.4×10^6 -
160 14.2×10^6 ton/a, with the mean being 5.7×10^6 ton/a (Fig. 2b). The sediment in the Qiantang
161 Estuary is mainly from the Changjiang Estuary. The huge sediment load from the Changjiang
162 River, used to be around 4.5×10^8 ton/a, is diffused southward and enters the Qiantang
163 Estuary - Hangzhou Bay system under the influence of the secondary Changjiang plume,
164 especially in winter when the northwesterly winds prevail and the waves are relatively strong
165 (Su and Wang, 1989; ECCHE, 1992; Fan et al., 2017; Dai, 2021).

166

167 **3. Data and method**

168 This study is based on three sets of data: bathymetry, water level and river discharge.

169 Bathymetry: Since the 1980s, the bathymetry in the estuarine reach has been measured
170 uninterruptedly during the spring tide of every April, July and November by the Zhejiang
171 Surveying Institute of Estuaries and Coasts (ZSIEC), representing bathymetries before (April)
172 and after (July) the high flow season and after autumn (November), the season when the
173 monthly maximum tidal ranges occur, respectively. The bed elevation along 60 cross-sections
174 was observed using an Odom Hydrotrac echo-sounder. The error of the measured bed level is
175 0.1 m. After each survey, the channel volumes below multi-year averaged high water levels

176 between cross-sections were calculated. The channel volumes of various sub-reaches and the
177 cross-sectional averaged elevations are collected from ZSIEC. The bed elevation before 2000
178 was with respect to the theoretically lowest astronomical tidal datum at Wusong, whereas the
179 subsequent surveys were with respect to the Chinese National Vertical Datum of 1985. In this
180 study the elevations are unified in accordance with the 1985 datum.

181 Water level: High and low water levels of each tide (twice a day) at the Zhakou, Yanguan
182 and Gaupu tidal gauging stations in the same period are collected from Zhejiang Hydrography
183 Bureau (ZHB). The Zhakou and Ganpu stations are the landward and seaward boundaries of
184 the estuarine reach of the Qiantang Estuary. Furthermore, the Ganpu station is the place where
185 the maximum tidal range along the Qiantang Estuary – Hangzhou Bay system occurs (Fig.
186 1b). The reach downstream from Ganpu is dominated by width convergence and the reach
187 upstream from Ganpu is dominated by bed friction. The Yanguan station is in the middle of
188 the estuarine reach. The distances from Yanguan to Zhakou and Ganpu are both about 50 km.

189 River discharge: Daily river discharge from Fuchun power station in the same period is
190 collected from ZHB as well.

191 Water levels in shallow channels are related to local geometry, such as width and depth.
192 Morphological evolutions in the Qiantang Estuary are extremely active and significantly
193 influence the water levels. To link the morphological evolution and river discharge variations,
194 relationships between the channel volumes of the two landward sub-reaches, e.g., the ZL and
195 LD reaches and the average river discharge of the four months before the bathymetrical
196 surveys are analyzed.

197 For the tidal dynamics analysis, the tidal range is determined as the difference between the

198 high and low water levels. The mid-water level is the average of the high and low water levels.
199 The tidal amplification factor is calculated as the ratio of the tidal ranges at Zhakou, at
200 Yanguan to those at Ganpu. This approach of analysis is similar but not identical to the
201 method of [Munk and Cartwright \(1966\)](#). Any changes in the tidal amplification factor provide
202 information on changes of the physical conditions within the estuary ([Wang et al., 2014, 2019;](#)
203 [Jalón-Rojas et al., 2018](#)). Especially, it can provide information of day-to-day changes.

204 For the seasonal and interannual tidal behavior analysis, we use the monthly averaged
205 high and low water levels, tidal ranges and amplification factors. To clarify the controlling
206 factors of water levels, the relationships between the tidal parameters at the upper stations and
207 various external forces are established, such as the channel volumes of the sub-reaches and
208 the tides at the seaward station Ganpu.

209 As tidal waves move into coastal and estuarine waters, a different high water propagation
210 speed than low water leads to tidal wave deformation ([Dronkers, 1986; Friedrichs and Aubrey,](#)
211 [1988](#)). A shallow basin tends to cause flood dominance and a deeper basin tends to cause ebb
212 dominance ([Friedrichs and Aubrey, 1994](#)). The tidal asymmetry is one of the factors
213 generating residual sediment transport and is associated with morphological development.

214 Tidal asymmetry is quantified using the method of [Friedrichs and Madsen \(1992\)](#):

$$215 \quad F = \frac{5}{3} \frac{A}{H} - \frac{b-B}{B} \quad (1)$$

216 in which, A is the tidal amplitude, H refers to cross-section averaged channel depth, b is the
217 total width (including tidal flats), and B is the width of the channel. If $F > 0$, the time variations
218 in channel depth are more important than time variations in channel width, leading to a

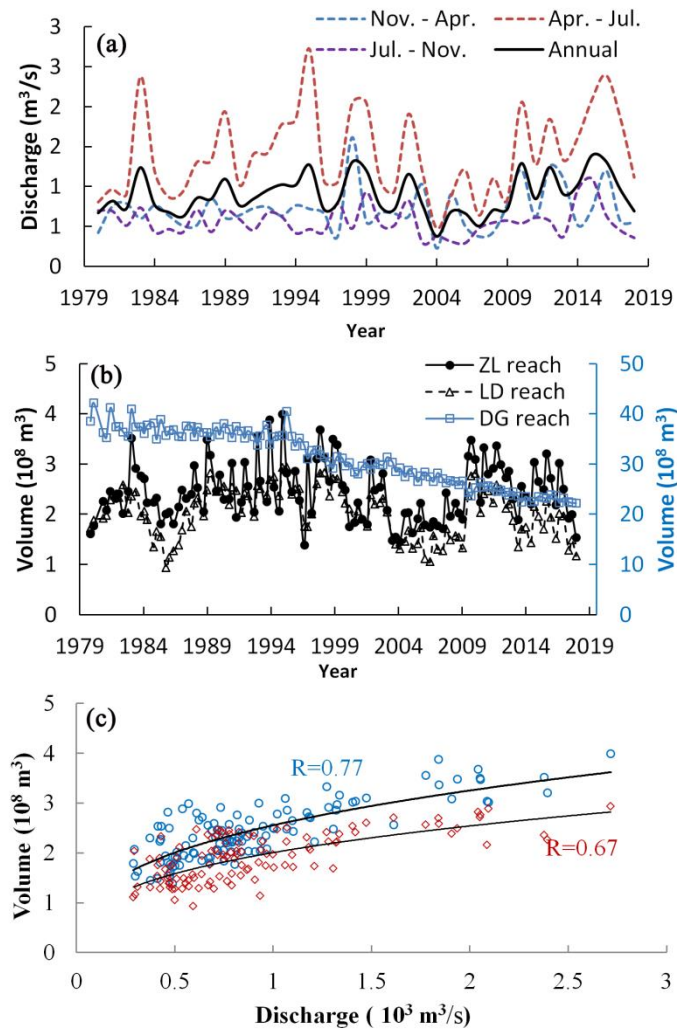
219 flood-dominant tide and a tendency for landward sediment transport; if $F < 0$, the opposite
220 holds, resulting in an ebb-dominant tide.

221

222 **4. Results**

223 **4.1 Morphological evolutions**

224 The morphological evolution of the estuary and its relationship with river discharge are
225 analyzed first, providing a basis for the tidal dynamics analysis. [Fig. 3](#) illustrates time series
226 of the average river discharge of the four months before each bathymetrical survey and the
227 channel volumes of the three sub-reaches in the months of April, July and November from
228 1980 to 2018. The annual averaged discharge varies between 370 m³/s and 1390 m³/s. Two
229 periods of continuous dry years (1980 - 1988 and 2003 - 2009), and two periods of continuous
230 wet years (1989 - 2002 and 2010 - 2018) can be roughly distinguished. In the dry years the
231 Qiantang River basin experienced relatively light precipitation whereas in the wet years it
232 received sufficient precipitation ([Xia et al., 2016](#)). The mean discharges of the four periods
233 are 801, 1022, 630 and 1123 m³/s, respectively. The average discharges of the periods before
234 the three bathymetrical surveys during 1980 - 2018 are 831, 1448 and 623 m³/s, respectively.
235 The discharges in the high flow seasons are larger than the bed formation discharge of the
236 Qiantang estuary, 1100 m³/s ([Chen et al., 2006](#); [Xie et al., 2017a](#)), and can amount to about
237 twice of those in the low flow seasons.



238

239 **Fig. 3.** (a) The average river discharge in the four months before the bathymetrical surveys in
 240 April, July and November, (b) the channel volumes below local annual highwater levels of the
 241 three sub-reaches of the estuary, (c) relationships of the channel volumes of the ZL and LD
 242 reaches and the average river discharge in the four months before bathymetric measurements.

243

244 The channel volumes of the ZL reach in April, July and November vary between $1.38 \times$
 245 10^8 and $3.16 \times 10^8 \text{ m}^3$, 1.54×10^8 and $3.99 \times 10^8 \text{ m}^3$, 1.45×10^8 and $3.00 \times 10^8 \text{ m}^3$,
 246 respectively, with the average being $2.22 \times 10^8 \text{ m}^3$, $2.79 \times 10^8 \text{ m}^3$ and $2.28 \times 10^8 \text{ m}^3$,
 247 respectively (Fig. 3b). The channel volumes of the LD reach in April, July and November
 248 vary between 0.93×10^8 and $2.60 \times 10^8 \text{ m}^3$, 1.14×10^8 and $2.93 \times 10^8 \text{ m}^3$, 1.11×10^8 and 2.47

249 $\times 10^8 \text{ m}^3$, respectively, with the average being $1.86 \times 10^8 \text{ m}^3$, $2.19 \times 10^8 \text{ m}^3$ and $1.72 \times 10^8 \text{ m}^3$,
250 respectively. Averagely, the channel volumes of the two sub-reaches in July are 20 - 25%
251 larger than in April and November. The channel volumes of both reaches correlate with the
252 average discharge prior to the bathymetrical surveys (Fig. 3c). This is consistent with the
253 findings of Xie et al. (2018) who found that channel volume upstream of Yanguan in July
254 correlates well with the river discharge between April and July. The cross-sectional area and
255 the cross-section averaged depth of estuaries are power functions of the river discharge
256 (Smith, 1974; Han et al., 2009). Since the mean river discharges during last November to
257 April and during July to November are comparable (Fig. 3a), overall, the channel volumes in
258 both reaches are also comparable in April and November. The high discharge from April to
259 July results in the largest channel volume in July. Furthermore, the channel volume -
260 discharge correlation for the ZL reach is better than for the LD reach, indicating that the role
261 of river discharge is more important in the upper reach. It should be noted that the channel
262 volume in July is mainly related to bed erosion caused by high discharge, especially by river
263 flood events, whereas in April and November the channel volume is related to accumulation
264 after a high flow season, due to sediment input by tidal currents (Han et al., 2003; Xie et al.,
265 2018). Moreover, the volume in April and November also depends on the channel volume of
266 last measurement. For example, the channel volume of the ZL reach in November 2010 is
267 $2.89 \times 10^8 \text{ m}^3$, much larger than the predicted value by the fitted curve in Fig. 3c, despite the
268 average discharge between August and November of 2010 is only $538 \text{ m}^3/\text{s}$. This is because
269 the channel volume in July 2010 is large, being $3.48 \times 10^8 \text{ m}^3$.

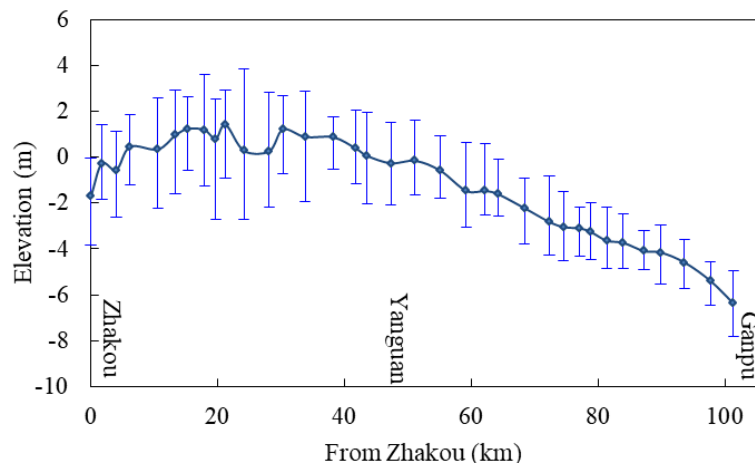
270 The average volumes of the ZL and LD reaches are 25% larger in the wet years than in

271 the dry years. For example, the averages volume of the ZL reach in the periods of 1980 - 1988,
272 1989 - 2002, 2003 - 2009 and 2010 - 2018 are 2.33×10^8 , 2.64×10^8 , 1.96×10^8 and $2.65 \times$
273 10^8 m³. Furthermore, extreme values of channel volumes can be observed. 1995 and 2004 are
274 the rainiest and driest years in the last decades, respectively (Lin et al., 2012; Xia et al., 2016).
275 As a result, extreme high and low annual river discharges occurred in the two years being
276 1390 and 370 m³/s, respectively. Correspondingly, the sum volumes of the two reaches in the
277 two years are largest and smallest, being 6.05×10^8 and 2.91×10^8 m³, respectively.

278 The seasonal and interannual variations in the channel volume of the DG reach are
279 opposite to the other two reaches. The average volumes of this reach in April, July and
280 November since 1980 are 31.14×10^8 , 30.37×10^8 and 31.55×10^8 m³, respectively. This is
281 related to the sediment exchange between the three sub-reaches. During the high discharge
282 periods, the sediment eroded from the ZL and LD reaches is transported seaward and
283 accumulated at the DG reach, and vice versa during the low discharge periods (Chen et al.,
284 1990; Han et al., 2003; Xie et al., 2018). The most remarkable change in the DG reach is that
285 the volume has been decreased continuously from 38.89×10^8 in 1980 to 22.24×10^8 m³ in
286 2018. This is related to the large-scale embankment project gradually implemented in the
287 Qiantang Estuary and Hangzhou Bay which has reduced the tidal prism of the estuary and
288 enhanced the sediment input (Han et al., 2003; Xie et al., 2021).

289 Fig. 4 shows the magnitudes of the cross-section averaged bed level changes of the
290 neighboring bathymetrical surveys since 1980. The changes in the ZL and LD reaches are
291 relatively large, varying between -3 and 3.5 m; those in the DG reach vary between -2 and 2.5
292 m. As previously reported (e.g., Chen et al., 1990; Xie et al., 2018), the local bed level

293 changes can be even larger than these cross-section averaged values.



294

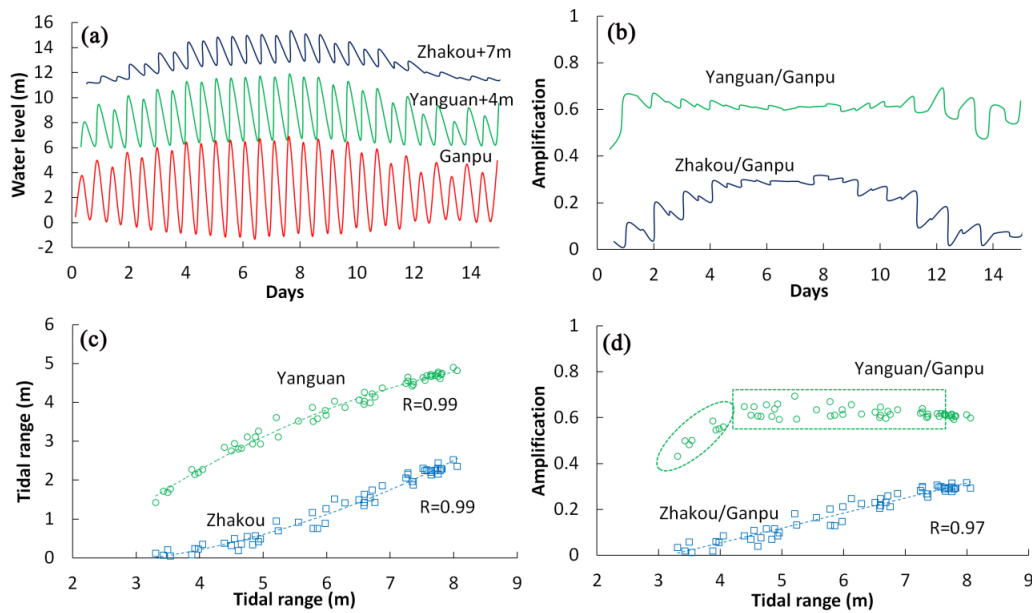
295 **Fig. 4.** The amplitudes of the cross-sectional bed level changes of the neighboring bathymetrical
296 surveys since 1980. The solid line denotes the longitudinal profile of the estuary, and the error bars
297 reflect the maximal bed erosion and accumulation.

298

299 **4.2 Temporal and spatial changes of tidal dynamics**

300 [Fig. 5](#) illustrates an example of fortnightly water levels at Zhakou, Yanguan and Ganpu
301 stations in October 2018. The monthly river discharge is $759 \text{ m}^3/\text{s}$, and no river flood events,
302 nor storm surge occurred. At the seaward station Ganpu, the high and low water levels vary
303 between 3.69 m and 6.90 m and between 0.47 m and -1.33 m, respectively. Accordingly, the
304 tidal range varies between 3.31 m and 8.06 m. At Yanguan, the highwater level varies
305 between 4.09 m and 7.73 m, whereas the variation of the low water level is insignificant,
306 fluctuating around 2.33 m with an amplitude of change less than 0.3 m. Accordingly, the tidal
307 range varies between 3.31 m and 4.90 m ([Fig. 5c](#)). According to [Talke and Jay \(2019\)](#), within
308 a tidal river, the lowest water levels occur during neap rather than spring tides, because a
309 larger tide increases the friction felt by river flow, and the point where the lowest low waters
310 begin to be during neap tides is the seaward boundary of the tidal river. Thus, the reach
311 upstream from Yanguan can be defined as a tidal river. The tidal range at Yanguan correlates

312 positively with the tidal range at Ganpu, whereas the amplification factor fluctuates around
 313 0.6 and is not influenced by the tidal range at Ganpu except that it increases with the tidal
 314 range at Ganpu during the neap tides (Fig. 5b, d). The high and low water levels at the
 315 landward station Zhakou vary between 4.12 m and 8.36 m, and between 4.19 m and 5.84 m,
 316 respectively. Both highest high and lowest low levels appear in the spring tides. The tidal
 317 range varies between 0.04 m and 2.52 m and the amplification factor varies between 0.01 and
 318 0.32, both correlating positively with the tidal range at Ganpu (Fig. 5c, d).

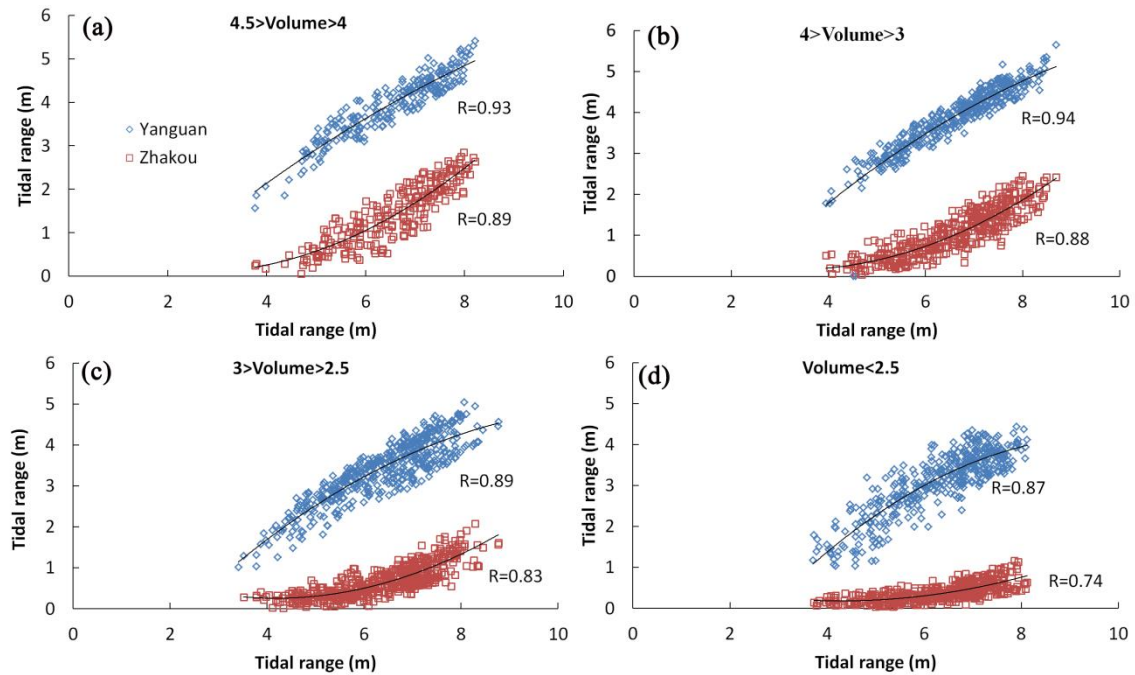


319
 320 **Fig. 5.** Time series of water levels at Zhakou, Yanguan and Ganpu in October 2018 (a), and the
 321 corresponding amplification factors (b). The relationships between the tidal ranges (c) and the
 322 amplifications (d) at Zhakou and Yanguan and the tidal range at Ganpu.

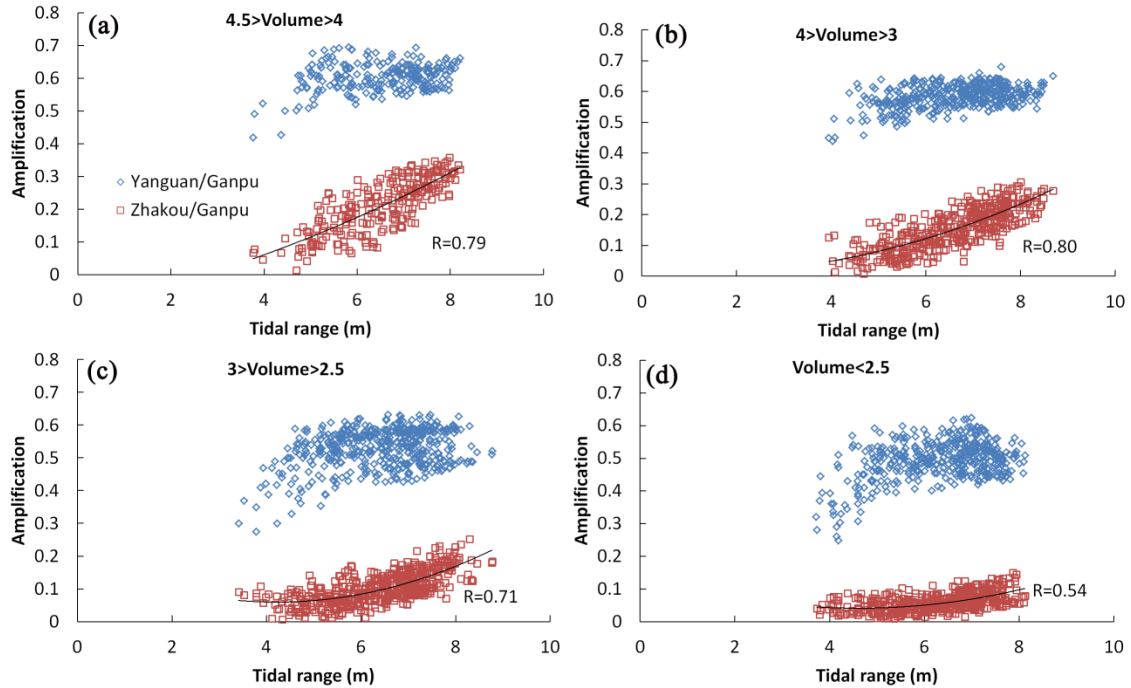
323

324 As morphology and river discharge also influence the tidal wave propagation, a longer -
 325 term comparison is made for different channel volume classes. The tidal ranges at the three
 326 stations in April, July and November since 1980 are chosen, matching the periods of the
 327 bathymetric data. River flood events can significantly influence water levels and morphology.
 328 To avoid this complication, for each channel volume class the tidal data during river flood

329 events are filtered out. Furthermore, the channel volume of the Zhakou - Yanguan reach is
 330 used since the channel volumes of the sub-reaches in the upper estuary show similar
 331 variations (Fig. 3). For the same channel volume class, the tidal ranges and the amplification
 332 factors correlate positively with the tidal range at Ganpu, except that the amplification at
 333 Yanguan fluctuates around a certain value if the tidal range at Ganpu is relatively large (Figs.
 334 6 and 7), consistent with the results of the fortnightly variations in Fig. 5. On the other hand,
 335 the larger the channel volume is, the larger the tidal ranges and amplifications in the upper
 336 estuary are. For example, under the tidal range at Ganpu of 8.0 m, the tidal range at Zhakou is
 337 2.55 m, 2.02 m, 1.71 m, 0.96 m, and the amplification is 0.32, 0.25, 0.21 and 0.12 for the
 338 various channel volume classes in decreasing order.



339
 340 **Fig. 6.** Relationships between the tidal ranges of Zhakou and Yanguan and the tidal range at
 341 Ganpu in various channel volume classes of the Zhakou - Yanguan reach. The unit of channel
 342 volumes is 10^8 m^3 , the same below.



343

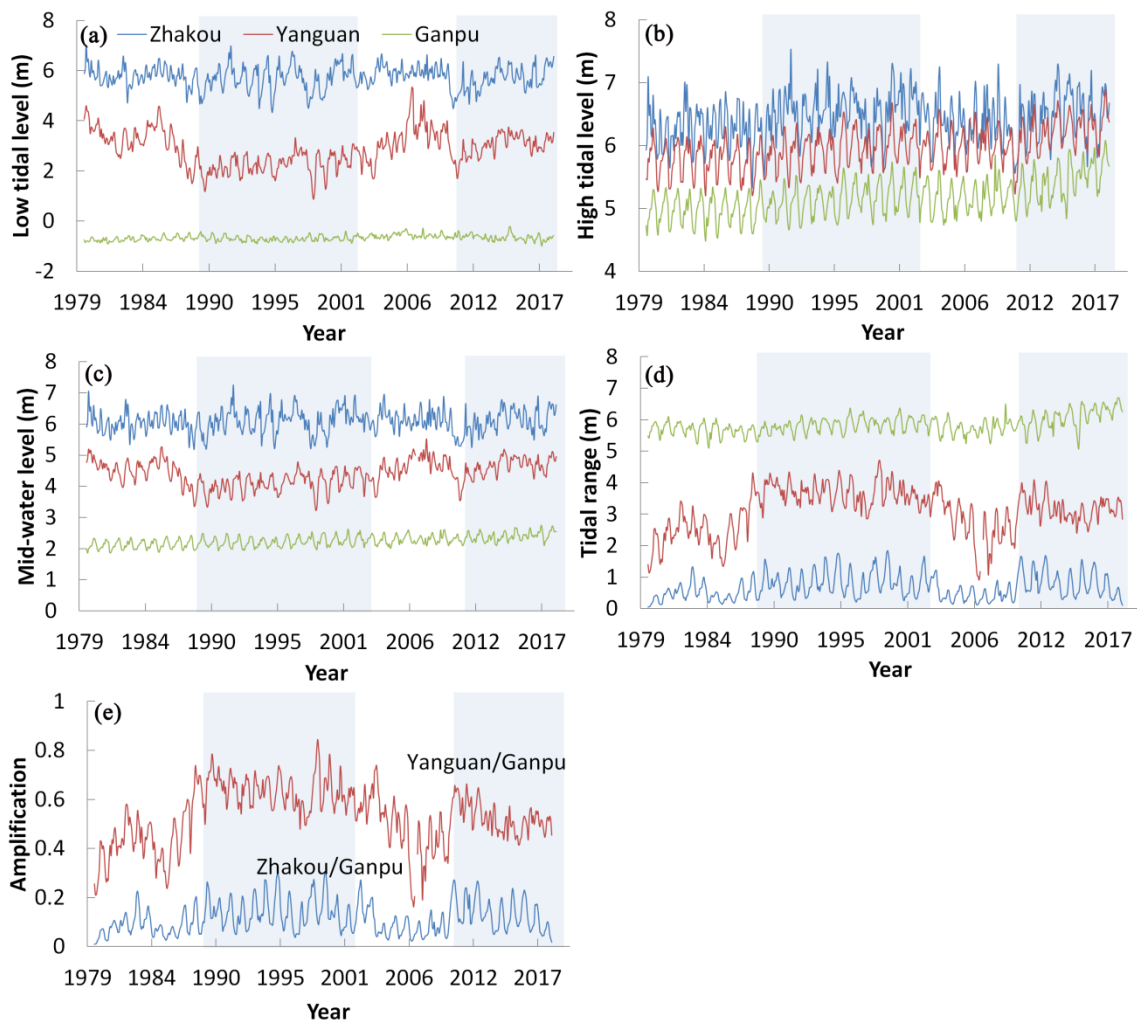
344 **Fig. 7.** Relationships between the amplification factor at Zhakou and Yanguan and the tidal range

345 at Ganpu in various channel volume classes of the Zhakou - Yanguan reach.

346

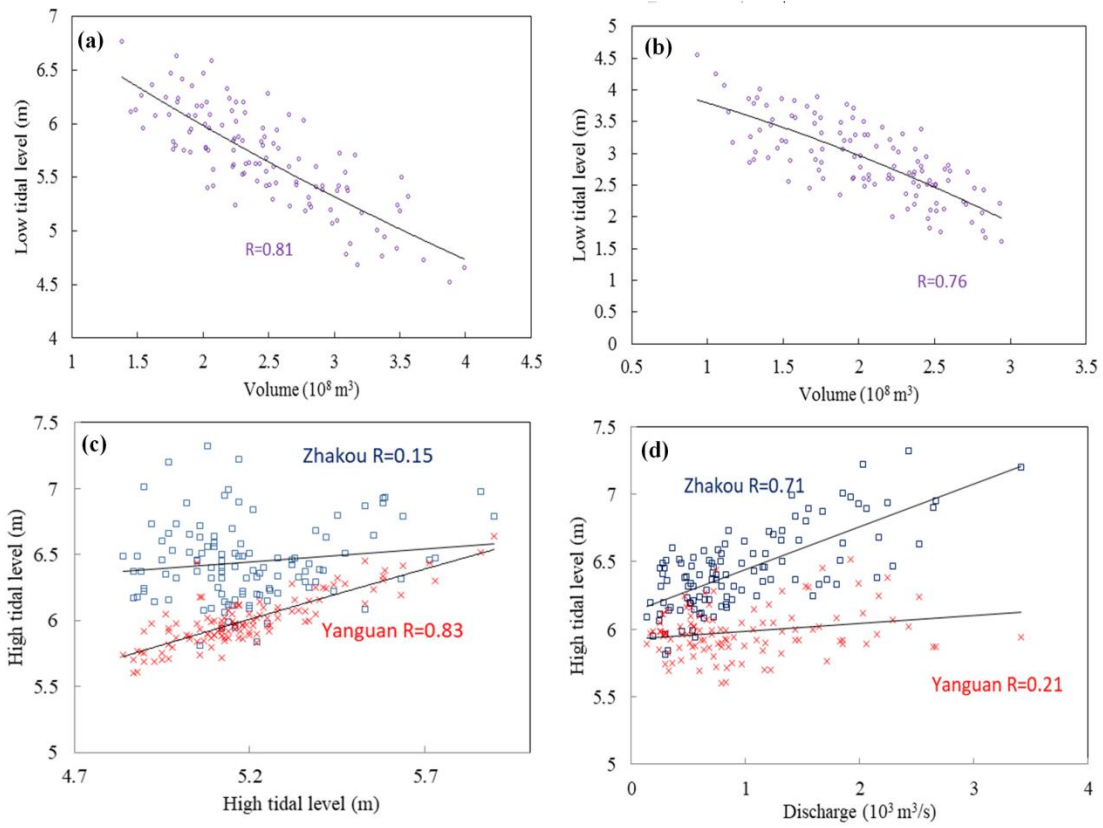
347 [Fig. 8](#) illustrates monthly average high, low and mid-water levels, tidal ranges at Zhakou,
 348 Yanguan and Ganpu and tidal amplifications at the former two stations. At Ganpu the
 349 variations of the monthly low level are limited, fluctuating around -0.60 m. The highwater
 350 level shows significant seasonal variations. Moreover, it shows an increasing trend, especially
 351 since 2007. The low level at Yanguan varies between 0.88 and 5.34 m, much more
 352 significantly than the low level at Ganpu. Most of the lowest low levels occur in July,
 353 corresponding to the maximum monthly river discharge which results in significant bed
 354 erosion. Furthermore, the low level is higher in the dry years than in the wet years. In the four
 355 periods of continuous dry and wet years, the mean low levels at Yanguan are 3.30, 2.26, 3.27
 356 and 3.02 m, respectively. The low water levels at Yanguan correlates with the channel volume

357 of the LD reach (Fig. 9), indicating that the low levels in the upper estuary depend on local
 358 bathymetries. The highwater level at Yanguan correlates with that of Ganpu whereas its
 359 relationship with the river discharge is insignificant (Fig. 9c, d). The low level at Zhakou
 360 varies between 4.33 and 6.97 m, showing the similar seasonal and interannual variations with
 361 that at Yanguan. The correlation between the low levels at Zhakou and the channel volume of
 362 the ZL reach is even better than at Yanguan (Fig. 9a). The highwater level at Zhakou depends
 363 on the variation of the river discharge whereas its relationship with the high level at Ganpu is
 364 insignificant.



365
 366 **Fig. 8.** The monthly low and highwater levels (a, b), mid-water levels (c), tidal ranges (d) at the
 367 three stations and the corresponding amplifications (e). The shades denote the continuous wet

368 years.



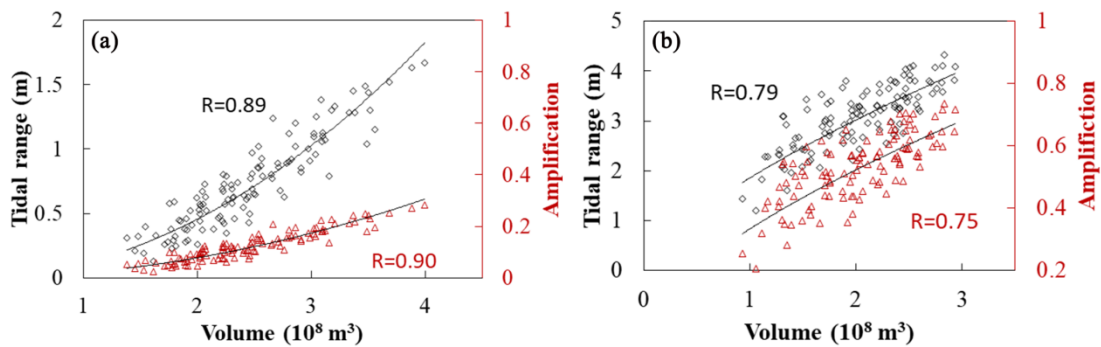
369

370 **Fig. 9.** Relationships between the monthly low water levels at Zhakou (a) and Yanguan (b) and
371 channel volumes of the ZL and LD reaches, respectively, and the monthly highwater levels at
372 Zhakou and Yanguan and highwater level at Ganpu (c) and the monthly river discharge (d),
373 respectively.

374

375 The mid-water levels and tidal ranges at the Yanguan and Zhakou also show significant
376 seasonal and interannual variations (Fig. 8c, d). The mean tidal range at Yanguan is 2.53 and
377 3.42 m in the periods of continuous dry and wet years, respectively. Accordingly, the mean
378 amplification factor is 0.45 and 0.58 in the periods of continuous dry and wet years,
379 respectively. Similarly, the mean tidal range at Zhakou is 0.44 and 0.82 m in the periods of

380 continuous dry and wet years, respectively. Accordingly, the mean amplification factor is 0.18
 381 and 0.24 in the periods of continuous dry and wet years, respectively. Overall, the
 382 amplification factors at the two stations in the wet years are about 30% larger than in the dry
 383 years. Both tidal ranges and amplifications at Zhakou and Yanguan correlate positively with
 384 the local channel volumes (Fig. 10).

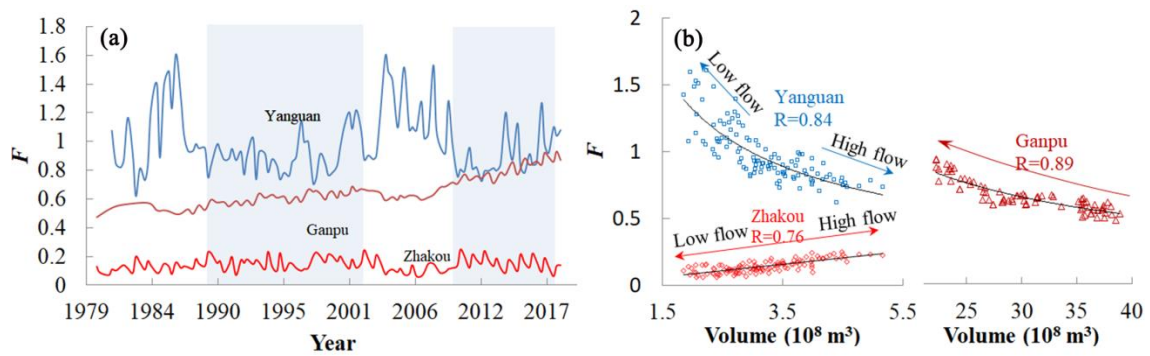


385
 386 **Fig. 10.** Relationships between monthly tidal ranges and amplifications at Zhakou (a) and
 387 Yanguan (b) and the channel volume of the ZL and LD reaches, respectively.

388

389 The metric of tidal asymmetry F at the three stations are positive, indicating that the tide
 390 in the estuary is flood dominant. At Ganpu F has increased from 0.47 to 0.87, with the most
 391 apparent increase occurring after 2007 (Fig. 11a), simultaneously with the increase of the
 392 highwater level. There exists good relationship between F and the local channel volume (Fig.
 393 11b). F at Yanguan varies between 0.62 and 1.61, with the average being 0.99, much larger
 394 than many other estuaries. For example, in the upper Pearl estuary in southern China, F is
 395 around 0.30 (Cao et al., 2020). The large F at Yanguan is related to the occurrence of the
 396 biggest tidal bore worldwide, which is an extreme case of tidal wave deformation. At Zhakou
 397 F varies between 0.06 and 0.25, with the average being 0.14. The tidal asymmetries at
 398 Yanguan and Zhakou show opposite relationship with the variations of river discharge. In the

399 low flow periods, F at Zhakou decreases while F at Yanguan increases, and vice versa in the
 400 high flow periods. In the high flow periods, the larger channel volume of the upper Qiantang
 401 Estuary results in an increase of tidal range at Zhakou and the landward penetration of the
 402 incoming tides. At Yanguan, the influence of the channel volume changes is relatively small.



403
 404 **Fig. 11.** Metric of tidal asymmetry F at the three stations in April, July and November since 1980
 405 (a), and the relationships between F and the channel volumes (b).

407 5 Discussion

408 5.1 The river-tide-morphology interaction

409 River-tide properties can vary in systems subject to strong fluctuations of river discharge.
 410 The effects of river flow on tidal dynamics are known, mostly based on analytical solutions or
 411 numerical models (Godin et al., 1991; Kukulka and Jay, 2003a, b; Jay et al., 2011; Sassi and
 412 Hoitink, 2013; Cai et al., 2015, 2020). There are basically four direct influences of high river
 413 discharge: (1) increased ebb currents, favoring the growth of overtides and causing tidal
 414 damping; (2) increased water levels and water depths, which means lowering the bed
 415 resistance; (3) changed hydraulic drag via changing of suspended sediment concentrations; (4)
 416 bed level change. Until recently, the impacts of river discharge on tidal decay and deformation
 417 were investigated using time series of real observations (Wang et al., 2014, 2019; Jalón-Rojas

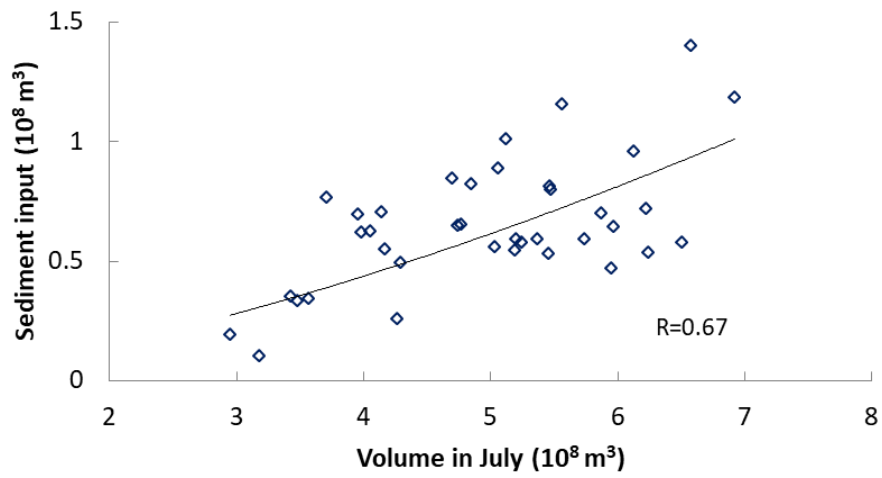
418 [et al., 2018](#)). Concerning tidal range and amplification, a higher river discharge corresponds
419 to a smaller tidal range and thus weaker amplification in the upper estuary. For example, the
420 tidal range in the upper Yangtze can be 1.7 to 7.5 times higher during dry periods than during
421 wet periods ([Guo et al., 2015](#)). Similar relations were found in the upper Scheldt Estuary and
422 the Gironde Estuary ([Wang et al., 2019](#); [Jalón-Rojas et al., 2018](#)). Because seasonal or
423 interannual morphological evolutions in most estuaries are insignificant unless the natural
424 systems are strongly disturbed by human activities, few have considered the role of natural
425 morphological evolutions on the tides. In fact, the erosion / accumulation rate of the Qiantang
426 Estuary is at least an order of magnitude greater than those documented from other
427 tide-dominated estuaries, where the evolution cycle takes place over decades ([Wang et al.,](#)
428 [2002](#); [Dalrymple and Choi, 2007](#); [van der Wal et al., 2002](#); [Wang et al., 2019](#); [Luan et al.,](#)
429 [2016](#); [Jalón-Rojas et al., 2018](#); [Cao et al., 2020](#)). It is necessary to consider the role of
430 morphological evolution on the tidal dynamics in the Qiantang Estuary.

431 In the Qiantang Estuary, the effects of river discharge in different reaches can be
432 different. The highwater level at Zhakou can be elevated by the high river discharge, but the
433 highwater level at Yanguan depends predominantly on the highwater level of the incoming
434 tides ([Fig. 8, 9](#)). At the upper reach, the high discharge induces significant bed erosion and
435 subsequently a larger channel volume. Correspondingly the low water levels at Zhakou and
436 Yanguan are lowered. The eroded sediments are transported seaward and accumulated at the
437 lower reach during a high discharge period. Thus, the low water levels at the two upstream
438 stations correlate with the local channel volumes ([Fig. 9a, b](#)), but their relationship with the
439 river discharge is insignificant. The high and low water levels at Ganpu are hardly influenced

440 by river discharge because of the larger width and depth (Fig. 8). The damping effect of high
441 river discharge on the tidal ranges at Zhakou and Yanguan is insignificant, probably because
442 the bed erosion by a high river discharge is fast. Bed erosion occurs basically synchronously
443 with river flood events. Meanwhile, the periods of river flood events of the Qiantang River
444 usually last several days to half month (Han et al., 2003; Xie et al., 2018). The damping effect
445 of high discharge on the tidal range was smoothed because we focused on the monthly
446 averaged data. The effect of tidal amplification induced by the high discharge is larger at the
447 upstream station than at the downstream station. The average tidal ranges at Zhakou and
448 Yanguan in the periods of continuous wet years are 1.86 and 1.35 times those in the periods of
449 continuous dry years, respectively (Fig. 8c).

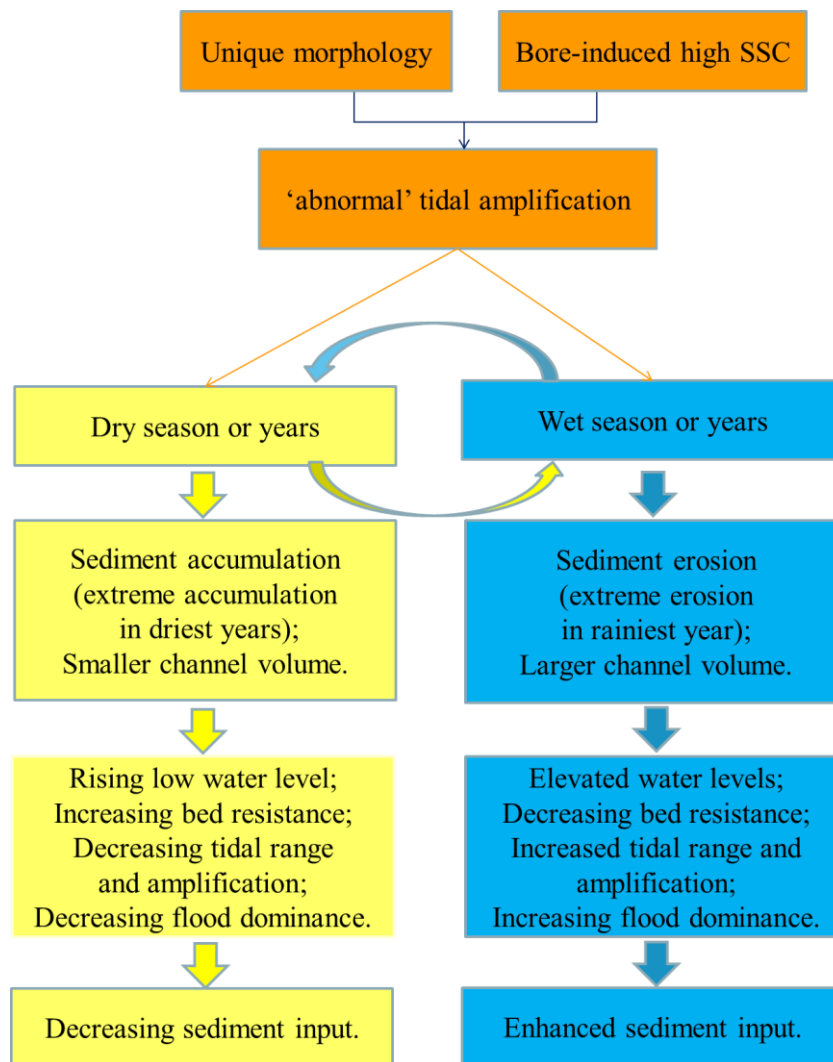
450 The low discharge during dry season or years exerts different effects from the high
451 discharge on the tidal dynamics. Under low discharge condition, sediment accumulation
452 occurs in the upper estuary because of the sediment input by tides, especially by the tidal bore
453 (Xie et al., 2018). Results in this study showed that the increased channel volumes upstream
454 Daquekou by the high river flow amplify the tide and enhance the flood dominance (Fig. 11),
455 favoring the sediment input after the high discharge period. A positive relationship exists
456 between the sediment accumulation from July to November and the sum volume of the ZL
457 and LD reaches in July (Fig. 12). Larger channel volumes in the two reaches mean a faster
458 sediment accumulation in the post high-discharge periods. With sediment accumulation in the
459 upper estuary, the low water levels increased accordingly, and the tidal amplification and
460 flood dominance decreased gradually. Subsequently, sediment input decreases gradually. Thus,

461 a dynamic morphodynamic equilibrium can be maintained. A conceptual model of the
462 river-tide-morphology interaction of the estuary is summarized in Fig. 13.



463

464 **Fig. 12.** The relationship between the sediment accumulation from July to November and the sum
465 volume in July in the ZL and LD reaches.



466

467 **Fig. 13.** A conceptual model of the river-tide-morphology interaction in the estuary.

468 The influences of human-induced morphological changes on tides have been evaluated in
 469 many estuaries. For example, mainly due to continuous channel deepening, the Ems Estuary
 470 experienced a tidal range increase of 125% at the mouth between 1950 (1.6 m) and 2010 (3.6
 471 m), and a transition of suspended sediment concentration from low ($\sim 1 \text{ kg/m}^3$) to high (>10
 472 kg/m^3) (van Maren et al., 2015; Winterwerp and Wang, 2013; Dijkstra et al., 2019). The tidal
 473 ranges of the upper region of the Pearl Estuary increased from 0.35 m in 1990 to 0.53 m in
 474 2005 due to the uncontrolled sand mining, enhancing the tidal dynamics (Zhang et al., 2010),
 475 but reducing the flood-dominant tidal asymmetry (Cao et al., 2020; Zhang et al., 2018). The

476 role of bed erosion by high river flow in the Qiantang Estuary is similar to the effect of
477 dredging and sand mining. However, the natural erosion of the Qiantang Estuary can be
478 gradually recovered in several months or years because of the ample sediment supply and the
479 strong tidal currents after the flood events. Human activities also exert influences on the
480 morphology of the Qiantang Estuary. Since the 1960s a large-scale embankment project has
481 been implemented seaward progressively, aiming at improving flood protection and
482 navigation (Han et al., 2003). Upstream Daquekou the embankment was basically finished
483 before the 1970s and the morphodynamic system has reached a new dynamic equilibrium (Han
484 et al., 2003; Xie et al., 2017b). The channel volumes in the ZL and LD reaches mainly depend
485 on the variations of the river discharge. The embankment in the DG reach was finished in the
486 2010s. The embankment decreases the tidal prism, enhances sediment accumulation and
487 hence the channel volume in this reach decrease continuously (Fig. 3b). The morphological
488 response still continues at present. The influence of the morphological evolution on the low
489 water level at Ganpu is insignificant. The highwater level has increased due to the enhanced
490 reflection of tidal wave by seawall (Han et al., 2003; Xie et al., 2017b; Zeng et al., 2017; Pan
491 et al., 2019). As a result, the tidal range at Ganpu has increased by about 0.5 m (Fig. 8).

492

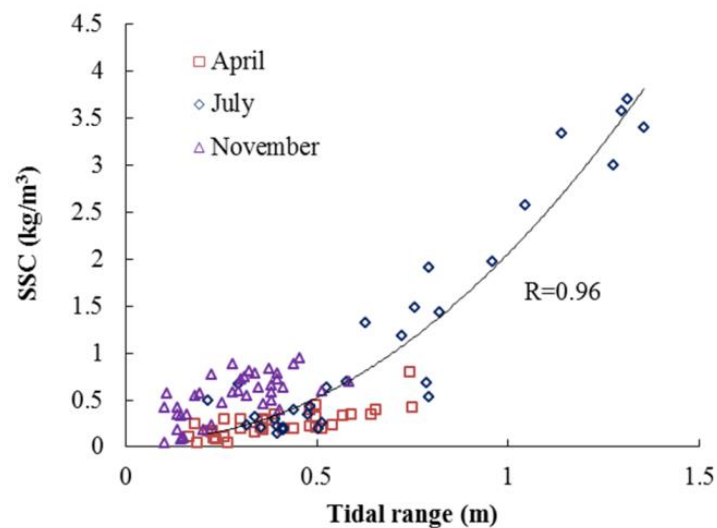
493 **5.2 Reasons for the ‘abnormal’ tidal amplification variations**

494 Usually, a larger tidal range in an estuary induces larger bed friction. Hence tidal
495 amplification at the upstream station correlates negatively with the tidal range at the
496 downstream station (Jalón-Rojas et al., 2018; Wang et al., 2019). In the Qiantang Estuary,
497 tidal amplifications at both Zhakou and Yanguan correlate positively with the tidal range at

498 Ganpu. This ‘abnormal’ tidal behavior is probably related to the unique hydrographic and
499 morphological characteristics of the estuary. The Yanguan reach is the place where the biggest
500 tidal bore in the world occurs, and current velocity can be as high as 6 m/s and strong
501 turbulence occurs. As a result, the suspended sediment concentration (SSC) during spring and
502 intermediate tides are large, with the maximal SSC more than 15 kg/m³ (Pan and Huang, 2010;
503 Tu and Fan, 2017). A high SSC can decrease the effective hydraulic drag (Winterwerp et al.,
504 2013; Wang et al., 2014). Furthermore, the larger the SSC, the more kinetic energy is
505 extracted from the water to be translated into potential energy, in order to maintain the high
506 SSC (Burchard and Schuttelaars, 2012; Li et al., 2018). Therefore, during spring and
507 intermediate tides, the increase of tidal amplification at Yanguan with the tidal range at Ganpu
508 is insignificant (Fig. 3b and Fig. 4).

509 At Zhakou, the tidal bore is weak. Only undular bore can be observed during spring tides
510 and no bore is formed during neap tides (Pan et al., 2007). Recent field work showed that the
511 maximal SSC in the upper estuary is 0.81, 3.7 and 0.95 kg/m³ in April, July and November of
512 2018, respectively (Fig. 14). In other words, the upper estuary is characterized by low
513 turbidity, comparable with other shallow systems. Therefore, the positive correlation between
514 the amplification at Zhakou and the tidal range at Ganpu cannot be explained by the SSC
515 effects. Instead, the abnormal amplification is probably related to the development of the
516 large longitudinal bar (Fig. 1b) and the variation of the water depth with the tidal range. The
517 bed elevation lowers landwards from 1 - 2 m at the bar apex at Qibao to around -2 m at
518 Zhakou. Under the annually average low water levels, the water depth appears smallest at
519 Yanguan, being 2.60 and increases landwards, being 7.89 m at Zhakou. The landward

520 increasing water depth in the Qiantang Estuary contrasts with the generally landward
521 decreasing trend in water depth (Cai et al., 2012; Hoitink and Jay, 2016; Wang et al., 2014;
522 Hoitink et al., 2017; Wang et al., 2019; Talke and Jay, 2019), and due to the development of
523 the large longitudinal bar (Fig. 1b), friction effects decrease with the water depth. Meanwhile,
524 the landward increase of water depth also reduces the hydraulic drag (Godin et al., 1991; Jay
525 et al., 2011; Wang et al., 2019).

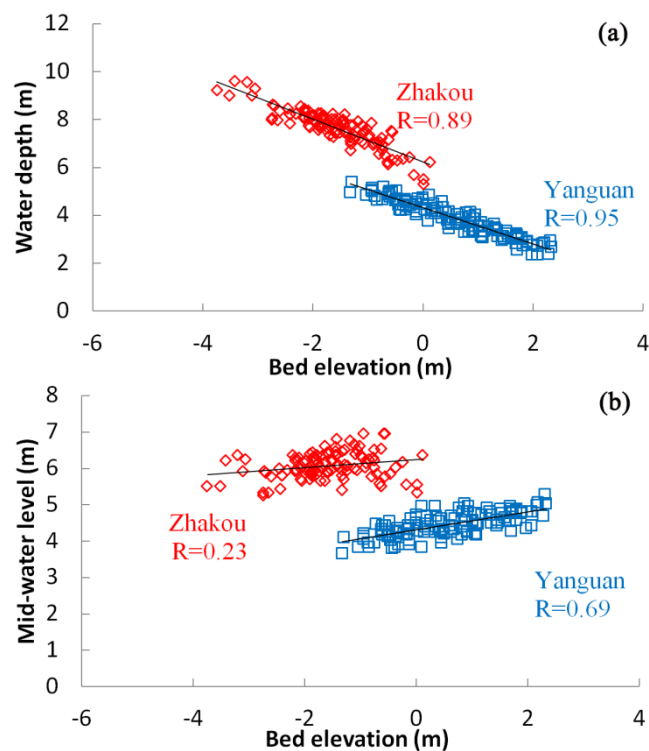


526
527 **Fig. 14.** The relationships between the maximal depth-averaged SSC at Qibao and tidal range at
528 Zhakou in April, July and November of 2018 (modified from Xie et al., 2020).

529
530 Talke and Jay (2019) identified two types of systems that are particularly prone to tidal
531 amplification: (a) shallow, strongly damped systems, in which a small increase in depth
532 produces a large decrease in effective friction, and (b) systems in which wave reflection and
533 resonance are strongly influenced by changes to depth, friction, and convergence. Apparently,
534 the Qiantang Estuary belongs to the former. During a short-term cycle with a normal
535 hydrograph, e.g., the spring-neap cycle, the morphological evolution is limited, but the water
536 depth increases with increasing tidal range because stronger tidal flow causes more resistance

537 to the river flow. The amplifications at Yanguan and Zhakou are determined by two different
538 physical mechanisms. At Yanguan the high SSC effect is more important, whereas at Zhakou
539 the effect of the variation of water depth in the upper estuary is dominant.

540 On the longer timescale, the morphological evolutions play an important role on the
541 amplification, especially due to the shallow depth. With the morphological evolutions in the
542 upper reach, the magnitudes of the monthly mean amplification factors at Zhakou and
543 Yanguan are 0.01 - 0.30 and 0.16 - 0.84, respectively. The bed level changes induced by the
544 variation of river flow induce the changes of water levels and amplification of the tidal ranges
545 (Fig. 8-10). Furthermore, the monthly water depths under mid-water levels in the upper
546 estuary correlate well with local bed elevations (Fig. 15). The increasing water depths with
547 the bed erosion by high flow reduce the hydraulic drag and favor the amplifications.



548
549 **Fig. 15.** Relationships between the cross-sectional water depths under the mid-water levels (a) and
550 the monthly mid-water levels (b) at Zhakou and Yanguan and their bed elevations.

551

552 **5.3 Implications**

553 In this study, we have evaluated the evolutions of vertical tides in the Qiantang Estuary. In
554 fact, the sediment transport and morphological evolution are mainly governed by horizontal
555 tides. However, the asymmetry of the vertical tide can be a good indicator of the asymmetry
556 of the horizontal tide (Wang et al., 2002; Zhou et al., 2018). As shown in Fig. 13, the SSC in
557 the upper estuary correlates well with the tidal range. Over the post high-flow periods, the
558 larger tidal range and tidal storage have contributed to an intensification of tidal pumping and
559 an increase of the SSC. Given that SSC decrease gradually upstream from Yanguan (Han et
560 al., 2003), it can be understood that the estuarine turbidity maximum shifts landwards. In turn,
561 during the low flow seasons or years, the tidal range and horizontal velocities decrease, and
562 the turbidity maximum shifts seawards. The cyclic seasonal and interannual transition of the
563 hydro-sedimentary conditions has profound consequences for the estuary, as high SSC is
564 associated with a strong reduction in oxygen levels (Uncles et al., 1998; Talke et al., 2009)
565 and primary production (Cloern, 1987; Kukulka and Jay, 2003a, b; Gao and Wang, 2008).

566 The present study has its methodological implications. Studies in recent years based on
567 analytical and numerical models (e.g., Kukulka and Jay, 2003a, b; Cai et al., 2012, 2015) or
568 on nonstationary harmonic methods (Guo et al., 2015, 2019; Cao et al., 2020) have largely
569 improved our understanding on the river-tide interaction. However, none of these studies
570 takes the joint effects of variations of river flow and morphology into account. Findings from
571 this study reveal that the tidal dynamics are sensitive to the seasonal and interannual
572 morphological changes in the Qiantang Estuary. At smaller timescales (e.g., spring-neap cycle)

573 the variation of SSC has significant influence on the tidal dynamics. This implies that
574 river-tidal dynamic models for this estuary must include sediment dynamics and
575 morphodynamics.

576

577 **6 Conclusions**

578 Based on long-term datasets of water levels at representative tidal gauging stations, river
579 discharge and bathymetrical data in the estuary, the temporal-spatial variations and controls of
580 the water levels were analyzed. The findings are summarized below.

581 (1) Within a spring-neap tidal cycle, tidal amplification in the upper estuary correlates
582 positively with the tidal range at the mouth, due to the high sediment concentration at the
583 middle reach and the variation of water depth in the upper reach.

584 (2) On the seasonal and interannual timescales, the direct influence of river discharge on the
585 tidal dynamics in the estuary is insignificant and restricted to elevating the highwater
586 level in the upper estuary. On the other hand, the variation of river discharge plays an
587 important indirect role on the tidal dynamics by triggering active morphological
588 evolutions.

589 (3) At the upper estuary, the tidal range and the amplification factor during high flow season
590 or years can be more than double of those during the low flow season or years. During the
591 low flow periods, the bed is gradually recovered, and the tidal range and amplification
592 decrease. The flood dominance increases and decreases in the high and low flow periods,
593 respectively. In the lower estuary, the flood dominance increases continuously, due to the
594 morphological response to the large-scale embankment project.

595 (4) A conceptual model of river-tide-morphology interaction under natural conditions is
596 proposed for estuaries with fast morphological evolutions.

597

598 **Acknowledgements:**

599 This research was financed by the National Natural Science Foundation of China (No.
600 41676085; 42176170; 42076178), the Zhejiang Provincial Hydraulic Science and Technology
601 Planning Project (No. RB2033), and the Dutch Royal Academy of Sciences via the project
602 Coping with Deltas in Transition (No. PSA-SA-E-02) within the framework of Program
603 Strategic Scientific Alliances between China and the Netherlands. We also wish to thank the
604 two anonymous reviewers for their constructive comments which improved this work greatly.

605

606 **References**

607 Bolle, A., Wang, Z.B., Amos, C.L., De Ronde, J., 2010. The influence of changes in tidal
608 asymmetry on residual sediment transport in the Western Scheldt. *Cont. Shelf Res.* 30(8),
609 871-882.

610 Burchard, H., Schuttelaars, H.M., 2012. Analysis of tidal straining as driver for estuarine
611 circulation in well-mixed estuaries. *J. Phys. Oceanogr.* 42 (2), 261-271.

612 Cai, H., Savenije, H.H.G, Yang, Q., Ou, S., 2012. Influence of river discharge and dredging
613 on tidal wave propagation: Modaomen Estuary case. *J. Hydraul. Eng.* 138, 885-96.

614 Cai, H., Savenije, H.H.G., Zuo, S., Jiang, C., Chua, V., 2015. A predictive model for salt
615 intrusion in estuaries applied to the Yangtze estuary. *J. Hydrol.* 529, 1336-1349.

616 Cai, H., Savenije, H. H. G., Garel, E., Zhang, X., Guo, L., Zhang, M., Liu, F., Yang, Q., 2020.

617 Seasonal behaviour of tidal damping and residual water level slope in the Yangtze River
618 estuary: identifying the critical position and river discharge for maximum tidal damping.
619 *Hydrol. Earth Sys. Sci.* 23, 2779-2794.

620 Cao, Y., Zhang, W., Zhu, Y., Ji, X., Xu, Y., Wu, Y., Hoitink, A.J.F., 2020. Impact of trends in
621 river discharge and ocean tides on water level dynamics in the Pearl River Delta. *Coast.*
622 *Eng.* 157, 103634.

623 Chen, J., Liu, C., Zhang, C., Walker, H., 1990. Geomorphological development and
624 sedimentation in Qiantang Estuary and Hangzhou Bay. *J. Coastal Res.* 6(3), 559-572.

625 Chen, S., Han, Z., Hu, G., 2006. Impact of human activities on the river reach in the Qiantang
626 Estuary (in Chinese with English abstract). *J. Sediment. Res.* 4, 61-67.

627 Choi, K., Kim, D., Jo, J., 2020. Morphodynamic evolution of the macrotidal Sittaung River
628 estuary, Myanmar: Tidal versus seasonal controls. *Mari. Geol.* 430, 106367.

629 Cloern, J. E., 1987. Turbidity as a control on phytoplankton biomass and productivity in
630 estuaries. *Cont. Shelf Res.* 7, 1367-1381.

631 Cooper, J.A.G., 2002. The role of extreme floods in estuary-coastal behaviour: contrasts
632 between river- and tide-dominated microtidal estuaries. *Sed. Geol.* 150, 123-137.

633 Dai, Z.J., 2021. Changjiang riverine and estuarine hydro-morphodynamic processes: in the
634 context of anthropocene era. Springer.

635 Dalrymple, R.W., Choi, K.S., 2007. Morphologic and facies trends through the fluvial-
636 marine transition in tide-dominated depositional systems: a schematic framework for
637 environmental and sequence-stratigraphic interpretation. *Earth Sci. Rev.* 81, 135-174.

638 Dijkstra, Y.M., Schuttelaars, H.M., Schramkowski, G.P., Brouwer, R.L., 2019. Modeling the

639 transition to high sediment concentrations as a response to channel deepening in the Ems
640 River Estuary. *J. Geophys. Res. Oceans* 124, 1578-1594.

641 Dronkers, J., 1986. Tide-induced residual transport of fine sediment. *Phys. Shall. Estua. Bay.*
642 228-244.

643 Editorial Committee for Chinese Harbors and Embayment (ECCHE), 1992. Chinese harbors
644 and embayment (Part V). China Ocean Press, Beijing (in Chinese).

645 Fan, D., Tu, J., Shang, S., Cai, G., 2014. Characteristics of tidal-bore deposits and facies
646 associations in the Qiantang Estuary, China. *Mar. Geol.* 348, 1-14.

647 Fan, D., Wu, Y., Zhang, Y., Burr, G., Huo, M., Li, J., 2017. South flank of the Yangtze Delta:
648 past, present, and future. *Mar. Geol.* 392, 78-93.

649 Friedrichs, C.T., Aubrey, D.G., 1988. Non-linear tidal distortion in shallow well-mixed
650 estuaries: a synthesis. *Estu. Coast. Shelf Sci.* 27(5), 521-545.

651 Friedrichs, C.T., Aubrey, D.G., 1994. Tidal propagation in strongly convergent channels. *J.*
652 *Geophys. Res.* 99, 3321-36.

653 Friedrichs, C., Madsen, O., 1992. Nonlinear diffusion of the tidal signal in frictionally
654 dominated embayments. *J. Geophys. Res.* 97 (N3C4), 5637-5650.

655 Gao, S., Wang, Y., 2008. Material fluxes from the Changjiang River and their implications on
656 the adjoining continental shelf ecosystem. *Cont. Shelf Res.* 28, 1490-1500.

657 Godin, G., 1991. Frictional effects in river tides, in *Progress in Tidal Hydrodynamics*. Edited
658 by BB Parker, John Wiley New York, pp. 379-402.

659 Guo, L., Van der Wegen, M., Jay, D.A., Matte, P., Wang, Z.B., Roelvink, D., He, Q., 2015.
660 River-tide dynamics: Exploration of nonstationary and nonlinear tidal behavior in the

661 Yangtze River estuary. *J. Geophys. Res. Oceans* 120, 3499-3521.

662 Guo, L., Wang, Z. B., Townend, I., He, Q., 2019. Quantification of tidal asymmetry and its
663 nonstationary variations. *J. Geophys. Res. Oceans* 124, 773-787.

664 Han, Z., Cao, Y., You, A., 2009. Verification of fluvio-morphology for macro-tide estuary with
665 tidal bore (in Chinese with English abstract). *Hydro-Sci. Eng.* 4, 83-90.

666 Han, Z., Dai, Z., Li, G., 2003. Regulation and Exploitation of Qiantang Estuary (in Chinese).
667 China Water Power Press, Beijing.

668 Hoitink, A.J.F., Jay, D.A., 2016. Tidal river dynamics: Implications for deltas. *Rev. Geophys.*
669 54, 240-272.

670 Hoitink, A.J.F., Wang, Z.B., Vermeulen, B., Huisman, Y., Kästner, K., 2017. Tidal controls
671 on river delta morphology. *Nature Geosci.* 10, 637-645.

672 Hu, P., Han, J.J., Li, W., Sun, Z.L, He, Z.G., 2018. Numerical investigation of a sandbar
673 formation and evolution in a tide-dominated estuary using a
674 hydro-sediment-morphodynamic model. *Coast. Eng. J.* 60(4), 466-483.

675 Huang, J.B., Xie, D.F., 2020. Detecting the river-sea influenced boundary changes in a
676 macro-tidal estuary based on morphodynamic modeling. *J. Coast. Res.* 104: 804-812.

677 Jalón-Rojas, I., Sottolichio, A., Hanquiez, V., Fort, A., Schmidt, S., 2018. To what extent
678 multidecadal changes in morphology and fluvial discharge impact tide in a convergent
679 (turbid) tidal river. *J. Geophys. Res. Oceans* 123, 3241-3258.

680 Jay, D.A., 1991. Green's law revisited: Tidal long-wave propagation in channels with strong
681 topography. *J. Geophys. Res.* 96(C11), 20585.

682 Jay, D.A., Leffler, K., Degens, S., 2011. Long-term evolution of Columbia River tides. *J.*

683 Water. Port Coast. Ocean Eng. 137(4), 182-191.

684 Kukulka, T., Jay, D. A., 2003a. Impacts of Columbia River discharge on salmonid habitat: 1.
685 A nonstationary fluvial tide model. J. Geophys. Res. 108(C9), 3293.

686 Kukulka, T., Jay, D. A., 2003b. Impacts of Columbia River discharge on salmonid habitat: 2.
687 Changes in shallow-water habitat. J. Geophys. Res. 108(C9), 3294.

688 Li, L., He, Z., Xia, Y., Dou, X., 2018. Dynamics of sediment transport and stratification in
689 Changjiang River Estuary, China. Estu. Coast. Shelf Sci. 213, 1-17.

690 Lin, C., Zhuo, H., Gao, S., 2005. Sedimentary facies and evolution in the Qiantang River
691 incised valley, eastern China. Mar. Geol. 219, 235-259.

692 Lin, S., Xu, Y.P., Tian, Y., Lou, Z.H., 2012. Spatial and temporal analysis of drought in
693 Qiantang River basin based on Z index and SPI (in Chinese with English abstract). J.
694 Hydroelec. Eng., 31(2), 20-26.

695 Luan, H.L., Ding, P.X., Wang, Z.B., Ge, J.Z., Yang, S.L., 2016. Decadal morphological
696 evolution of the Yangtze Estuary in response to river input changes and estuarine
697 engineering projects. Geomorphology 265, 12-23.

698 Matte, P., Secretan, Y., Morin, J., 2014. Temporal and spatial variability of tidal-fluvial
699 dynamics in the St. Lawrence fluvial estuary: an application of nonstationary tidal
700 harmonic analysis. J. Geophys. Res. Oceans 119, 5724-44.

701 Munk, W.H., Cartwright, D.E., 1966. Tidal spectroscopy and predication. Philos. Trans. R.
702 Soc. Lond. Ser. A. 259, 533-581.

703 Pan, C., Lin, B., Mao, X., 2007. Case Study: Numerical Modeling of the Tidal Bore on the
704 Qiantang River, China. J. Hydraul. Eng. 133(2), 130-138.

705 Pan, C., Zheng, J., Chen, G., He, C., Tang, Z., 2019. Spatial and temporal variations of tide
706 characteristics in Hangzhou Bay and cause analysis (in Chinese with English Abstract).
707 Ocean Eng. 37(3), 1-11.

708 Pan, C., Huang, W., 2010. Numerical modeling of suspended sediment transport in Qiantang
709 River: An estuary affected by tidal bore. J. Coast. Res. 26, 1123-1132.

710 Postma, H., 1961. Transport and accumulation of suspended matter in the Dutch Wadden Sea.
711 Neth. J. Sea Res. 1 (1-2), 148-190.

712 Sassi, M.G., Hoitink, A.J.F., 2013. River flow controls on tides and tide-mean water level
713 profiles in a tidal freshwater river. J. Geophys. Res. Oceans 118, 4139-4151.

714 Savenije, H.H.G., 2012. Salinity and tides in alluvial estuaries, completely revised 2nd edition,
715 www.salinityandtides.com.

716 Shaw, J.B., Mohrig, D., 2014. The importance of erosion in distributary channel network
717 growth, Wax Lake Delta, Louisiana, USA. Geology 42(1), 31-34.

718 Shimosono, T., Tajima, Y., Akamatsu, S., Matsuba, Y., Kawasaki, A., 2019. Large-scale
719 channel migration in the Sittang River Estuary. Sci. Rep. 9, 9862.

720 Smith, T.R., 1974. A derivation of the hydraulic geometry of steady-state channels from
721 conservation principles and sediment transport laws. J. Geol. 82 (1), 98-104.

722 Song, D., Wang, X.H., Zhu, X., Bao, X., 2013. Modeling studies of the far-field effects of
723 tidal flat reclamation on tidal dynamics in the East China Seas. Estuar. Coast. Shelf Sci.
724 133, 147-160.

725 Su, J.L., Wang, K.S., 1989. Changjiang river plume and suspended sediment transport in
726 Hangzhou Bay. Cont. Shelf Res. 9, 93-111.

727 Syvitski, J.P.M., Kettner, A.J., Overeem, I., Hutton, E.W.H., Hannon, M.T., Brakenridge, G.R.,
728 Day, J., Vörösmarty, C., Saito, Y., Giosan, L., Nicholls, R.J., 2009. Sinking deltas due to
729 human activities. *Nat. Geosci.* 2 (10), 681-686.

730 Talke, S.A., Jay, D.A., 2019. Changing tides: The role of natural and anthropogenic factors.
731 *Ann. Rev. Mar. Sci.* 12, 14.1-14.31.

732 Talke, S.A., De Swart, H.E., De Jonge, V.N., 2009. An idealized model and systematic
733 process study of oxygen depletion in highly turbid estuaries. *Estu. Coast.* 32, 602-620.

734 Tian, Y., Xu, Y.P., Booij, M.J., Lin, S.J., Zhang, Q.Q., Lou, Z.H., 2012. Detection of trends
735 in precipitation extremes in Zhejiang, east China. *Theor. Appl. Climatol.* 107, 201-210.

736 Toublanc, F., Brenon, I., Coulombier, T., Le Moine, O., 2015. Fortnightly tidal asymmetry
737 inversions and perspectives on sediment dynamics in a macrotidal estuary (Charente,
738 France). *Cont. Shelf Res.* 94, 42-54.

739 Tu, J., Fan, D., 2017. Flow and turbulence structure in a hypertidal estuary with the world's
740 biggest tidal bore. *J. Geophys. Res. Oceans* 122(4), 3417-3433.

741 Uncles, R.J., Joint, I., Stephens, J.A., 1998. Transport and retention of suspended particulate
742 matter and bacteria in the Humber-Ouse Estuary, United Kingdom, and their relationship
743 to hypoxia and anoxia. *Estuaries* 21, 597-612.

744 Van der Wal, D., Pye, K., Neal, A., 2002. Long-term morphological change in the Ribble
745 estuary, Northwest England. *Mar. Geol.* 189, 249-266.

746 Van Maren, D.S., Winterwerp, J.C., Vroom, J., 2015. Fine sediment transport into the
747 hyper-turbid lower Ems River: The role of channel deepening and sediment-induced drag
748 reduction. *Ocean Dyn.* 65(4), 589-605.

749 Wang, Z.B., Jeuken, M.C.J.L., Gerritsen, H., de Vriend, H.J., Kornman, B.A., 2002.
750 Morphology and asymmetry of the vertical tide in the Westerschelde estuary. *Cont. Shelf*
751 *Res.* 22(17), 2599-2609.

752 Wang, Z.B., Vandenbruwaene, W., Taal, M., Winterwerp, H., 2019. Amplification and
753 deformation of tidal wave in the Upper Scheldt Estuary. *Ocean Dyn.* 69, 829-839.

754 Wang, Z.B., Winterwerp, J.C., He, Q., 2014. Interaction between suspended sediment and
755 tidal amplification in the Guadalquivir Estuary. *Ocean Dyn.* 64, 1487-1498.

756 Winterwerp, J.C., Wang, Z.B., Van Brackel, A., Van Holland, G., Kösters, F., 2013.
757 Man-induced regime shifts in small estuaries-II: a comparison of rivers. *Ocean Dyn.* 63,
758 1293-1306.

759 Winterwerp, J.C., Wang, Z.B., 2013. Man-induced regime shifts in small estuaries-I: Theory.
760 *Ocean Dyn.* 63(11-12), 1279-1292.

761 Xia, F., Liu, X., Xu, J., Xu, L., Shi., Z., 2016. Precipitation change between 1960 and 2006 in
762 the Qiantang River basin, East China. *Climat. Res.* 67, 257-269.

763 Xie, D., Gao, S., Wang, Z.B., Pan, C., Wu, X., Wang, Q., 2017a. Morphodynamic modeling of
764 a large inside sandbar and its dextral morphology in a convergent estuary: Qiantang
765 Estuary, China. *J. Geophys. Res. Earth Surf.* 122, 1553-1573.

766 Xie, D., Pan, C., Wu, X., Gao, S., Wang, Z.B., 2017b. Local human activities overwhelm
767 decreased sediment supply from the Changjiang River: Continued rapid accumulation in
768 the Hangzhou Bay-Qiantang Estuary system. *Mar. Geol.* 392, 66-77.

769 Xie, D., Pan, C., Gao, S., Wang, Z.B., 2018. Morphodynamics of the Qiantang Estuary, China:
770 Controls of river flood events and tidal bores. *Mar. Geol.* 406, 27-33.

771 Xie, D.F., Huang, J., Jiang, B., Li, R., Tang, Z., Lu, H., 2020. A preliminary study on seasonal
772 variations of sediment concentrations in the inner Qiantang Estuary. *IOP Conf. Ser. Earth*
773 *Environ. Sci.* 569.

774 Xie, D.F., Wang, Z.B., van der Wegen, M., Huang, J., 2021. Morphodynamic modeling the
775 impact of large-scale embankment on the large bar in a convergent estuary. *Mar. Geol.*
776 442(2), 106638.

777 Yu, Q., Wang, Y., Gao, S., Flemming, B., 2012. Modeling the formation of a sand bar within a
778 large funnel-shaped, tide-dominated estuary: Qiantangjiang Estuary, China. *Mar. Geol.*
779 299-302, 63-76.

780 Zeng, J., Chen, G., Pan, C., Zhang, Z., 2017. Effect of dike adjustment on the tidal bore in the
781 Qiantang Estuary, China. *J. Hydrodyn.* 27(3), 452-459.

782 Zeng, J., Sun, Z.L., Pan, C.H., Chen, G., 2010. Long-periodic feature of runoff and its effect o
783 riverbed in Qiantang estuary (in Chinese with English abstract). *J. Zhejiang Uni. (Eng.*
784 *Sci.)* 44(8), 1584-1588.

785 Zhang, M., Townend, I., Zhou, Y., Cai, H., 2015a. Seasonal variation of river and tide energy
786 in the Yangtze estuary, China. *Earth Surf. Proc. Land.* 41(1), 98-116.

787 Zhang, W., Cao, Y., Zhu, Y., Zheng, J., Xu, Y., Wu, Y., Hoitink, A.J.F., 2018. Unravelling the
788 causes of tidal asymmetry in deltas. *J. Hydrol.* 564, 588-604.

789 Zhang, W., Ruan, X., Zheng, J., Zhu, Y., Wu, H., 2010. Long-term change in tidal dynamics
790 and its cause in the Pearl River Delta, China. *Geomorphology* 120 (3-4), 209-223.

791 Zhang, X., Dalrymple, R.W., Yang, S.Y., Lin, C.M., Wang, P., 2015b. Provenance of
792 Holocene sediments in the outer part of the paleo-Qiantang River estuary, China. *Mar.*

- 793 Geol. 366, 1-15.
- 794 Zhou, Z., Coco, G., Townend, I., Gong, Z., Wang, Z.B., Zhang, C.K., 2018. On the stability
795 relationships between tidal asymmetry and morphologies of tidal basins and estuaries.
796 Earth Surf. Process. Land., 43(9), 1943-1959.